

FEBRUARY 23 2023

# Experimental investigation on the enhancement of plenum window noise reduction using solid scatterers

Xiao-Long Li; Wai Kit Lam; S. K. Tang 



*J Acoust Soc Am* 153, 1361 (2023)

<https://doi.org/10.1121/10.0017353>



View  
Online



Export  
Citation

CrossMark

## Related Content

Acoustical Plenum Chambers

*J Acoust Soc Am* (June 2005)

The influence of plenum geometry toward engine performance at BM student formula car

*AIP Conference Proceedings* (July 2020)

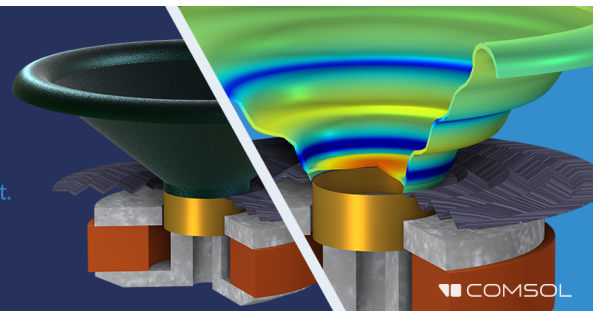
Acoustic design of wall, ceiling, and plenum for college buildings.

*J Acoust Soc Am* (October 2010)


## Take the Lead in Acoustics

The ability to account for coupled physics phenomena lets you predict, optimize, and virtually test a design under real-world conditions – even before a first prototype is built.

» Learn more about COMSOL Multiphysics®



# Experimental investigation on the enhancement of plenum window noise reduction using solid scatterers

Xiao-Long Li,<sup>1,a)</sup> Wai Kit Lam,<sup>2</sup> and S. K. Tang<sup>3,b)</sup> 

<sup>1</sup>Faculty of Architecture and Urban Planning, Chongqing University, Chongqing, China

<sup>2</sup>Department of Building Environment and Energy Engineering, The Hong Kong Polytechnic University, Hong Kong, China

<sup>3</sup>School of Engineering, The University of Hull, Hull HU6 7RX, United Kingdom

## ABSTRACT:

The sound transmission across plenum windows installed with rigid non-resonant cylindrical scatterer arrays was investigated in detail using scale-down model measurements carried out inside a fully anechoic chamber. The arrays have manifested to some extent the acoustical behaviors of virtual sonic crystals. The maximum cross section blockage ratio was 0.6. The effects of plenum window gap, array configuration, and scatterer diameter on the sound transmission characteristics were also examined. Results indicate that the window cavity longitudinal modes and the gap modes control the sound transmission characteristics at low frequencies. The upper bound of this frequency range increases with decreasing gap width. Within this frequency range, the scatterers have negligible effect on the sound transmission. At higher frequencies, the array configurations with scatterer(s) attached to the window walls result in stronger sound reduction. There are relatively higher sound transmission loss improvements around the frequencies where a full bandgap is observed. There are wide bandgaps in various lattice directions, and the present results suggest that they play a role in the broadband improvement of sound reduction. © 2023 Author(s). All article content, except where otherwise noted, is licensed under a Creative Commons Attribution (CC BY) license (<http://creativecommons.org/licenses/by/4.0/>). <https://doi.org/10.1121/10.0017353>

(Received 29 October 2022; revised 4 February 2023; accepted 6 February 2023; published online 23 February 2023)

[Editor: Ning Xiang]

Pages: 1361–1374

## I. INTRODUCTION

Traffic noise has long been one of the major environmental hazards that is a threat to public health.<sup>1,2</sup> Its mitigation in residential areas is of particular importance because residential environments, both indoor and outdoor, can have strong restorative power on human beings. There is always a need for strong and effective noise reduction devices for residential building applications.

Residential buildings within urbanized areas are in high demand because of convenience and easy access to resources. Ground traffic is the major source of noise pollution in these areas. As urban areas are always congested, traditional noise mitigation measures, such as roadside noise barriers<sup>3</sup> and building clustering,<sup>4</sup> are ineffective if not impossible. Measures that can be adopted on building façades are then a focus. However, balconies are not effective noise screening devices unless sound absorption is applied.<sup>5</sup> Double glazing windows<sup>6</sup> are strong noise reduction devices, but they jeopardize natural ventilation, resulting in unacceptable indoor air quality unless mechanical ventilation systems are in place. This is undesirable as these ventilation systems are going to consume extra electrical energy and have adverse impacts on sustainability development. A noise reduction device that can offer strong acoustical protection and at the

same time allow for an acceptable level of natural ventilation is urgently needed.<sup>7</sup>

Tang and co-workers have recently carried out an extensive study on the traffic noise protection that can be provided by plenum windows.<sup>8–10</sup> A plenum window is a partially opened double glazing window, but the size of the opening and the gap distance between the two glass panes are much larger than those of Kerry and Ford.<sup>11</sup> Since then, this window type has attracted the attention of many researchers, for instance, Yu *et al.*<sup>12</sup> and Du *et al.*<sup>13</sup> There are worldwide efforts focusing on strengthening the sound reduction of plenum windows. Typical examples include the installation of sound absorbers (both oblique porous materials<sup>13</sup> and transparent micro-perforation sheets<sup>14</sup>) and scatterers<sup>15,16</sup> into the window void.

Both the two-dimensional numerical study of Tang<sup>15</sup> and the experimental study of Lee *et al.*<sup>16</sup> demonstrate that sound scatterer arrays are very useful for improving the noise reduction of a plenum window without much reduction of natural ventilation effectiveness and daylight penetration. A detailed experimental investigation is carried out in the present study to understand how non-resonant scatterers and their arrangements can strengthen traffic noise reduction. Effort is also made to understand how the spectral characteristics of the sound transmission across plenum windows are affected by the scatterers.

## II. EXPERIMENTAL SETUP

The experiment in the present study was carried out inside the fully anechoic chamber of the Hong Kong

<sup>a)</sup>Also at: Key Laboratory of New Technology for Construction of Cities in Mountain Area, Ministry of Education, Chongqing University, Chongqing, China.

<sup>b)</sup>Electronic mail: S.Tang@hull.ac.uk

Polytechnic University. The working dimension of the chamber is  $4.5\text{ m} \times 4\text{ m} \times 5\text{ m}$  (height). The reverberation times (RTs) above the 200 Hz one-third octave band are below 0.1 s. The experimental condition was essentially a free field one, which resembles those in actual practice (for instance, Li *et al.*<sup>10</sup>).

### A. The scale model and the sound source

A 1:4 scale-down model resembling that of Tong and Tang<sup>8</sup> was adopted in the present study. Figure 1 illustrates the model, its dimensions, and the related nomenclature. This model was a box made of 18 mm thick acoustically hard varnished plywood without any parallel surfaces. The model plenum window was installed on the vertical wall of the model. Its length ( $L$ ) and height ( $H$ ) were fixed at 500 and 260 mm, respectively. The outer and inner opening widths ( $w$ ) were also fixed at 167 mm. The height and the opening widths were so chosen to align with those of the practical plenum window.<sup>10</sup> Perspex panels of 3 mm thickness were used to mimic the glass panes of the practical plenum window. The gap width  $G$  does vary in practice. In principle, the narrower the gap, the higher the traffic noise reduction.<sup>8</sup> In this study, three gap widths were adopted. They were 98, 158, and 218 mm.

The scatterers adopted in the present study were cylindrical aluminum rods with diameter,  $d$ , of 10, 19, and 32 mm. It is not desirable to put many scatterers into the plenum window void as it has been shown by Tang<sup>15</sup> that the noise reduction improvement will not be significant if the rows of the scatterer array exceed two. Also, the air movement will be much hindered if too many scatterers are installed.

A total of 11 scatterer array arrangements are included in the present study and are summarized in Fig. 2. The separation distances between scatterers are also given in Fig. 2. These arrangements can be basically classified into three types, namely, the “regular,” “single staggered,” and “dual staggered.” The latter two array types could result in higher noise reduction than that of the former one as shown by Tang.<sup>15</sup> In all these arrangements, the first row of scatterers is located at the entrance of the overlapping region.

The regular type, which is presented in Figs. 2(a)–2(e), consists of scatterers positioned symmetrically about the plenum window central plane. The single staggered type arrays adopted in the present study are shown in Figs. 2(f)–2(i). They consist of only one scatterer row offset from the window central plane. The last type, the dual staggered type, is made up of two offset scatterer rows as indicated in Figs. 2(j) and 2(k). For the sake of easy reference, the abbreviation  $V(m,n)$  represents hereinafter a regular scatterer array with  $m$  rows and  $n$  columns of scatterers. As discussed above,  $m \leq 2$  in the present study. Symbols “s” and “ds” are added to the abbreviation to indicate “single staggered” and “dual staggered” array, respectively. For the single staggered type, an additional number is added behind “s” to indicate which scatterer row is offset. For example, “s1” denotes that the first scatterer row is offset, and so on. A summary of these abbreviations is given in Fig. 2.  $V(0,0)$  denotes the plenum window without scatterers.

The sound source in the present study was a linear loudspeaker array made up of twenty 6-in. aperture loudspeakers capable of producing sound from 80 Hz to 25 kHz. The total length of this linear loudspeaker array source was 3.2 m, which was much longer than the width of the outer opening of the model plenum window (167 mm). This setup resembles that of Tong and Tang<sup>9</sup> for traffic noise reduction study. A similar approach of using a loudspeaker/tweeter array is quite common in traffic noise scale model studies, for instance, El Dien and Woloszyn.<sup>17</sup> In the present experiment, the sound source was located at a horizontal distance of 1 m away from the model and was set parallel to the model receiver room façade on which the model plenum window was installed. The horizontal centreline of the model plenum window was 0.5 m from the anechoic chamber floor. The effect of ground reflection in the anechoic chamber was negligible.

The RTs inside the model receiver room were measured by six microphones [1/4-in. Brüel & Kjær (Nærum, Denmark) type 4951] spanned over the entire volume of the receiver room using the maximum length sequence (MLS) approach implemented by DIRAC.<sup>18</sup> The sound source was an 8-cm aperture tweeter located at a corner of the receiver

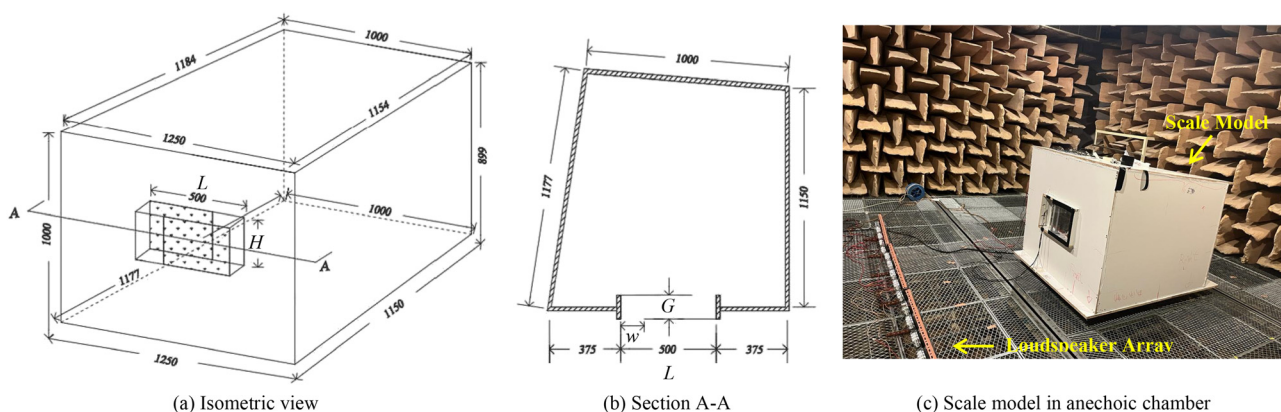


FIG. 1. (Color online) The scale model and nomenclature (all dimensions in mm). (a) Isometric view; (b) horizontal cross section; (c) the scale model setup in the anechoic chamber.

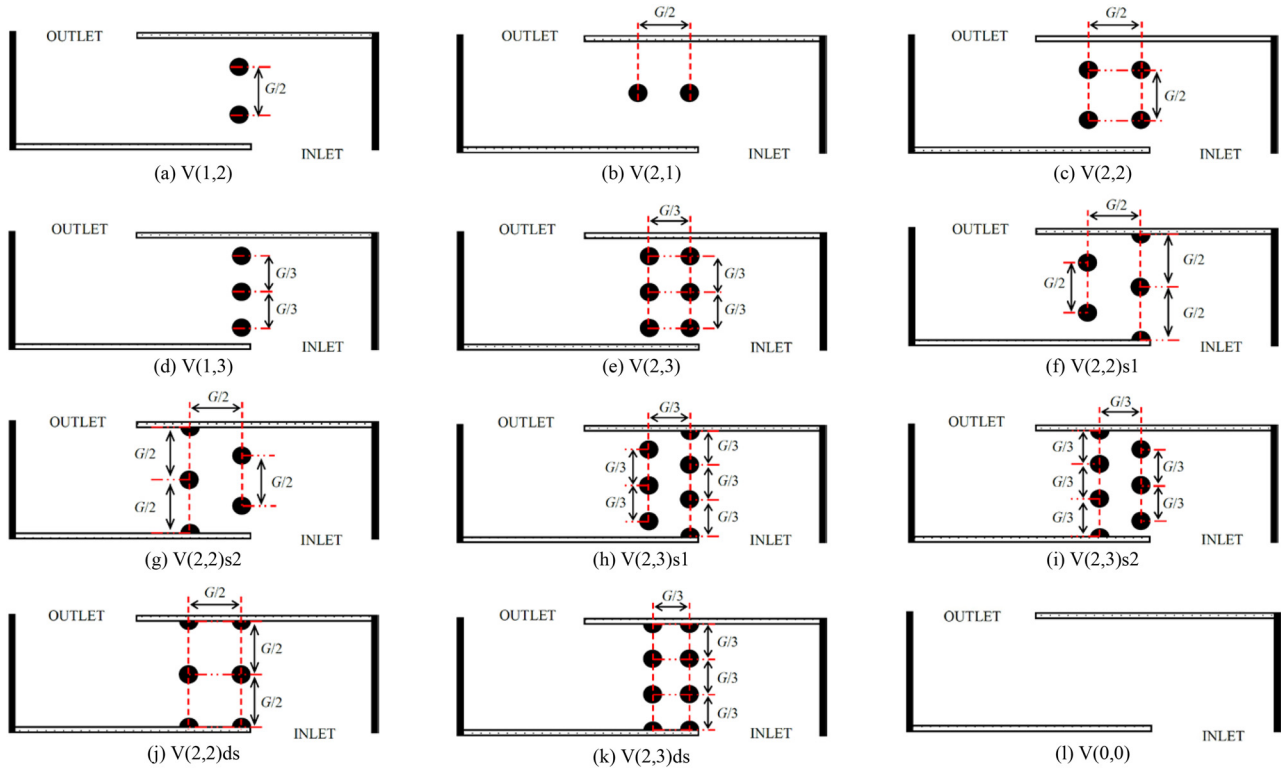


FIG. 2. (Color online) Forms of scatterer arrays included in the present study.

room. Two corners were chosen in the measurement. The model receiver room was very reverberant as shown in Fig. 3. Although there are some changes in the low frequency RTs when the window gap width  $G$  is altered, it can be observed that the change of RTs due to the installation of the cylinder arrays is insignificant, and the size of the cylindrical scatterer does not have much effect on the RTs. There are RT dips around the 250 and 315 Hz one-third octave bands for all cases tested in the present study. It is believed to be due to the longitudinal standing waves along the window length. As the model receiver room is sufficiently reverberant for sound transmission loss (TL) measurement, the RTs and the dips are, therefore, not discussed further.

A flanking transmission test was carried out by covering the plenum window firmly by hard plywood before the experiments. Results show that the average sound level inside the model receiver room is at least 30 dB below that of the incident sound over the frequency range of interest (not shown here). Flanking transmission can, thus, be ignored.

## B. Measurement procedure

The sound TL of the plenum window  $V(m,n)$ ,  $TL_{mn}$ , can be estimated by using average noise level inside the receiver room ( $SPL_{rec}$ ) and that at the window outdoor inlet ( $SPL_{in}$ ),<sup>19</sup>

$$TL_{mn} = SPL_{in,mn} - SPL_{rec,mn} + 10 \log_{10} \left( \frac{S_w}{RC_{mn}} \right), \quad (1)$$

where  $RC$  is the room constant of the receiver room and  $S_w$  the area of the plenum window facing the incoming sound.

$SPL_{rec}$  was measured by six 1/4-in. Brüel & Kjær type 4951 microphones inside the receiver room located based on the requirement of BS ISO 10140-2.<sup>20</sup>  $SPL_{in}$  was measured by three such microphones equi-spaced on the vertical center-line of the window inlet plane. The sound measurement for each plenum window was done simultaneously using the Brüel & Kjær type 3506D PULSE data recorder with a rate of 65 536 samples/s/channel. White noise signal was fed to the linear loudspeaker array during each sound TL measurement.

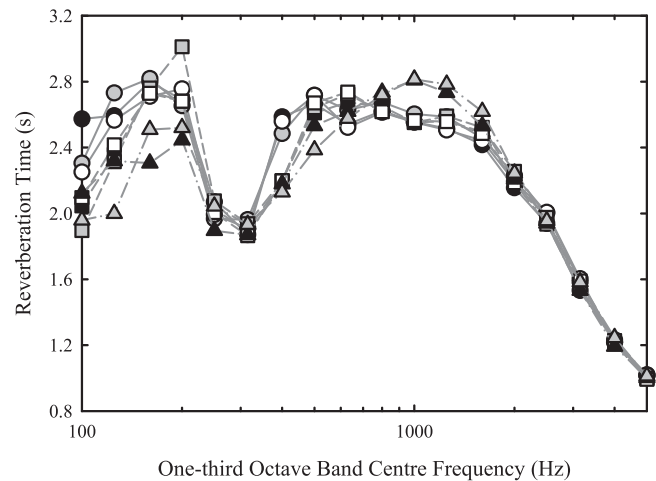


FIG. 3. Reverberation times inside the model receiver room. ●,  $V(0,0)$ ,  $G = 218$  mm; ○,  $V(2,3)$ ,  $G = 218$  mm,  $d = 10$  mm; ■,  $V(0,0)$ ,  $G = 158$  mm; □,  $V(2,3)$ ,  $G = 158$  mm,  $d = 10$  mm; ▲,  $V(0,0)$ ,  $G = 98$  mm; △,  $V(2,3)$ ,  $G = 98$  mm,  $d = 19$  mm.



The sound TL improvement due to the installation of the  $m \times n$  cylinder array,  $\Delta TL_{mn}$ , is, as the RTs are not much affected by the array,

$$\Delta TL_{mn} = TL_{mn} - TL_{00} \approx SPL_{rec,00} - SPL_{rec,mn}. \quad (2)$$

As traffic noise is always a concern, it is worthwhile to express the broadband sound TL as a single A-weighted rating relevant to traffic noise.<sup>8,9</sup> The normalized traffic noise spectrum<sup>21</sup> is adopted for such purpose in this study. A similar estimation procedure has also been applied by researchers, for instance, Tong and Tang<sup>8</sup> and Garai and Guidorzi.<sup>22</sup> The traffic noise TL of  $V(m,n)$ ,  $TL_{tr,mn}$ , is given by the expression

$$TL_{tr,mn} = 10 \log_{10} \left( \frac{\sum_{i=1}^{18} 10^{0.1(N_i - TL_{mn,i})}}{\sum_{i=1}^{18} 10^{0.1N_i}} \right), \quad (3)$$

where subscript  $i$  denotes the  $i$ th one-third octave band and  $N_i$  the traffic noise spectrum weighting of that frequency band. The change in the traffic noise TL by installing the cylinder array is simply taken to be

$$\Delta TL_{tr,mn} = TL_{tr,mn} - TL_{tr,00}. \quad (4)$$

### III. BAND STRUCTURES OF SCATTERER ARRAYS

Although the scatterer arrays adopted in the present study are not of infinite length, the multiple reflections from the two windowpanes that form the air passage within the plenum window help create virtual sonic crystal structures

within the window void.<sup>23</sup> It is, therefore, beneficial to examine the theoretical band structures of these scatterer arrays before analysing the experimental results. The lattice constant  $l_c$  and the area of the unit cell  $A_c$  of each of these structures depend on  $m$  and  $n$  and will vary even for a fixed array form when  $G$  is changed. For a regular array form, such as  $V(2,2)$ ,  $V(2,2)ds$ ,  $V(2,3)$ , and  $V(2,3)ds$ ,  $l_c = G/n$ , and the unit cell is a square of side  $l_c$ . The Bragg interference frequencies,  $f_{B\alpha}$ , and the filling fraction  $\sigma$  are, respectively,<sup>24</sup>

$$f_{B\alpha} = \alpha \frac{c}{2l_c} = \alpha \frac{nc}{2G} \text{ and } \sigma = \frac{\pi d^2}{4A_c} = \frac{\pi d^2}{4l_c^2} = \frac{\pi n^2}{4} \left( \frac{d}{G} \right)^2, \quad (5)$$

where  $c$  is the ambient speed of sound, and  $\alpha$  is an integer. Although  $f_{B\alpha}$  corresponds to the case of normal sound incidence, it is still relevant to the overall sound power transmission direction within the window void ( $\Gamma X$  in Fig. 4).

The situation becomes complicated for the staggered or non-square array forms. Figure 4 summarizes the types of unit cells involved in the present study and the windows associated with each of them. The lattice information and the first irreducible Brillouin zones of the rectangular sonic crystal lattices [Figs. 4(a) and 4(b)] are well known (for instance, Miyashita<sup>23</sup>) and need no further description. However, the lattice shown in Fig. 4(c), which corresponds to the arrays with single staggered scatterer arrangement, has a unit cell that is not a regular hexagon as in that of Lagarrigue *et al.*<sup>25</sup> It is of rhombic shape, and the irreducible Brillouin zone has four corners.<sup>26</sup> The area of the unit cell is the same as that of the square one, and thus,  $\sigma$  of the staggered and the square scatterer array patterns will be the same if  $G$  and  $d$  are fixed.

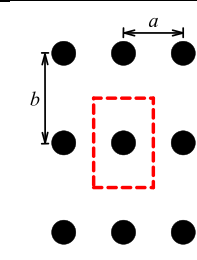
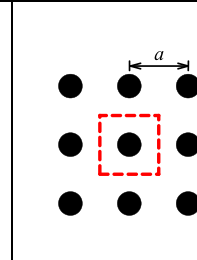
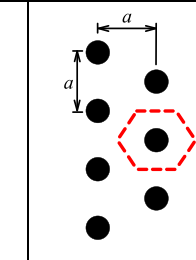
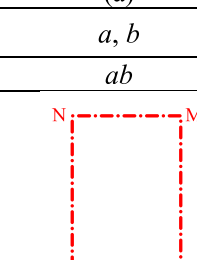
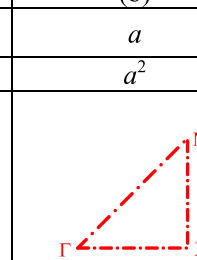
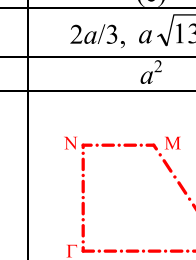
Sonic crystal lattice			
Side length(s) of unit cell	$a, b$	$a$	$2a/3, a\sqrt{3}/6$
Unit cell area, $A_c$	$ab$	$a^2$	$a^2$
Irreducible Brillouin zone			
Window & scatterer array	$V(2,1)$	$V(2,2), V(2,2)ds, V(2,3), V(2,3)ds$	$V(2,2)s1, V(2,2)s2, V(2,3)s1, V(2,3)s2$

FIG. 4. (Color online) Virtual sonic crystal lattice information. (a) Rectangular; (b) square; (c) rhombic. Dashed line, unit cell boundary; dashed-dotted line, Brillouin zone.

The spectral performance of the plenum windows after the installation of the scatterer arrays will depend on the window cavity modes, the bandgaps of the scatterer arrays, and the filling fraction (which is basically the blockage ratio). Although the sonic crystal effect is weaker as the number of scatterer rows decreases (for  $m \leq 5$ ),<sup>27</sup>  $m$  is kept not more than 2 in the present study as a compromise for better air movement as discussed in Tang.<sup>15</sup> It can also be inferred from the numerical results of Tang<sup>15</sup> that the TL improvement resulting from arrays with a small number of scatterers will not be significant. Therefore, only the band structures of the V(2,2) and V(2,3) series will be examined in this section. The associated eigenfrequencies are determined by solving the Helmholtz equation within the unit cells with the Floquet periodic boundary conditions using the finite-element method.<sup>28</sup> For easy presentation, the frequencies presented hereinafter are all scaled back to those of the real full size practical plenum windows.

The band structures of the scatterer arrays installed in the window V(2,3) with square unit cells in the present study are presented in Fig. 5. The abscissa of Fig. 5 is associated with the corners of the Brillouin zones (Fig. 4). The bandgap centre frequency  $f_{B\alpha}$  increases with decreasing  $G$  for a fixed array form. Similar to the experimental results of Sánchez-Pérez *et al.*,<sup>27</sup> the width of the bandgap in the  $\Gamma X$  direction (normal incidence direction) increases when  $d$  is increased for a fixed  $G$ . For  $G = 218$  or  $158$  mm, the results with  $d = 10$  mm are not significant and, thus, are not presented in Figs. 5(a) and 5(b) for the sake of visual clarity.

No complete bandgap is observed for  $G = 218$  mm. However, one can observe from Fig. 5(a) that there is a small but clear  $\Gamma X$  direction bandgap at  $\sim 590$  Hz ( $f_{B1}$ ), and the bandgap width increases with  $d$ . For the V(2,3) window with  $G = 218$  mm, bandgaps in the  $\Gamma X$  and  $XM$  directions can be observed as frequency increases. One can observe a more organized  $\Gamma X$  bandgap at  $\sim 1600$  Hz, which is close to  $f_{B3}$ , for  $d = 32$  mm. Near to  $f_{B2}$ , bandgaps can be found in the  $XM$  direction, but they are relatively narrow.

For window V(2,3) with  $G = 158$  mm, the band structures are very similar to those of the case with  $G = 218$  mm, except that the band frequencies are higher, and a narrow but complete bandgap is observed for  $d = 32$  mm at around 2400 Hz [Fig. 5(b)]. Apart from the  $\Gamma X$  direction bandgap near to  $f_{B1}$ , similar bandgaps are observed at frequencies above 2000 Hz and even up to around 4000 Hz for  $d = 19$  and 32 mm, but no such gap can be seen for  $d = 10$  mm (not presented here).

When  $G$  is reduced to 98 mm, there is no bandgap in any direction apart from the one near to  $f_{B1}$  for  $d = 10$  mm [Fig. 5(c)]. However, one can find quite a number of  $\Gamma X$  direction bandgaps at higher frequencies when  $d$  is increased to 19 mm. A complete bandgap, although very narrow, is observed in this case at  $\sim 4000$  Hz. The associated  $\Gamma X$  direction bandgap width is comparable to that at  $f_{B1}$ . Together with the results for  $G = 158$  mm, it appears that complete bandgap is possible when the filling fraction exceeds 0.265. As the major sound propagation direction across the windows is  $\Gamma X$ , the bandgaps in the  $XM$  direction could be less significant. Also, the scattering at  $\sim f_{B1}$  could have been

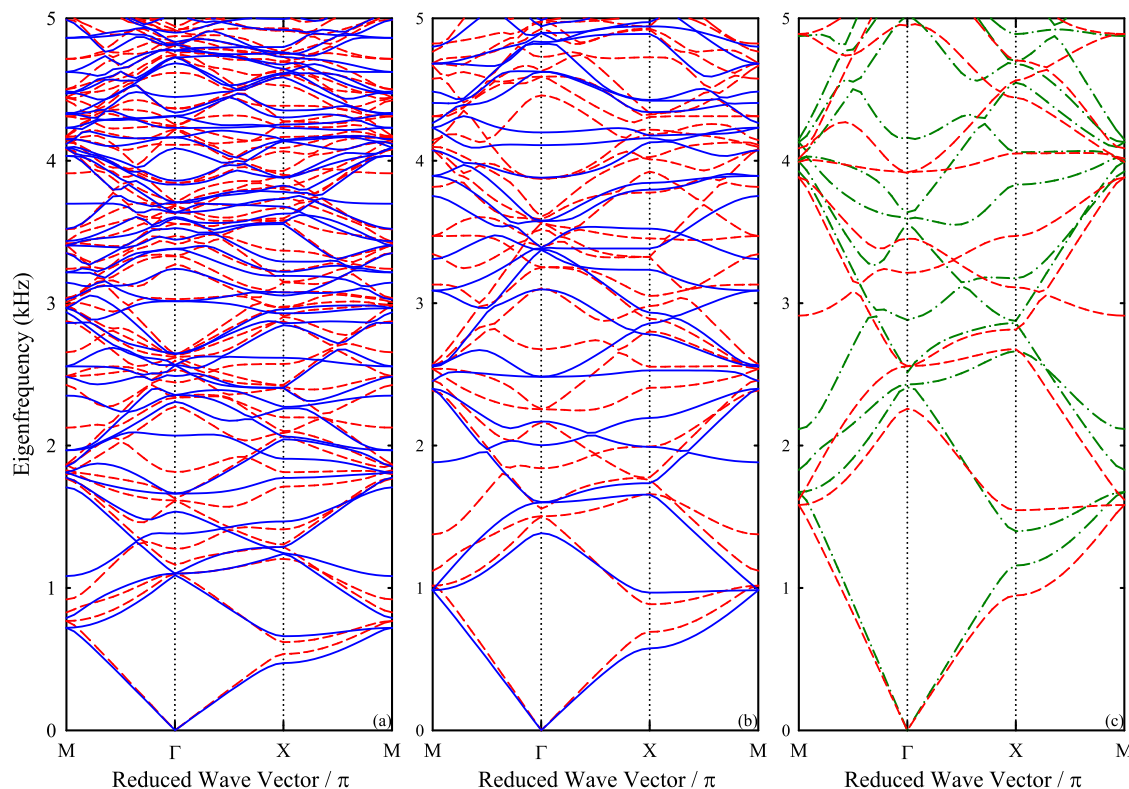


FIG. 5. (Color online) Band structures of the virtual sonic crystals in V(2,3) with square unit cells. (a)  $G = 218$  mm; (b)  $G = 158$  mm; (c)  $G = 98$  mm. Solid line,  $d = 32$  mm; dashed line,  $d = 19$  mm; dashed-dotted line,  $d = 10$  mm.

affected by the lower order window normal cavity modes. More discussions will follow in Sec. IV.

The band structure patterns of the scatterer arrays in V(2,2) with square unit cells are basically the same as those for the V(2,3) cases, except that the band frequencies are lower, and no complete bandgap is found, probably because of the lower filling fraction. They can roughly be retrieved by applying a factor of 2/3 to the eigenfrequency axis of Fig. 5. Therefore, they are not presented.

Figure 6 illustrates the band structures of the V(2,3) virtual sonic crystals with the rhombic unit cells [Fig. 4(c)]. Complete bandgaps are found even when  $G = 218$  mm in this case with  $d = 32$  mm [Fig. 6(a)]. For  $G = 218$  mm, no obvious complete bandgaps at frequency above 1000 Hz can be observed as in the square lattice case, but some bandgaps in the NM, MX, and  $\Gamma$ N directions can clearly be noticed at frequencies below 2500 Hz. There is also a very narrow bandgap in the  $\Gamma$ X direction at around 1000 Hz.

Complete bandgaps are clearly observed as  $G$  is reduced, and the bandgaps in the NM, MX,  $\Gamma$ X, and  $\Gamma$ N directions become wider at the same time [Figs. 6(b) and 6(c)]. They should lead to more broadband TL improvement than that at  $G = 218$  mm. Again, the band structures of the single staggered cases of the V(2,2) series can be easily inferred from results of the staggered V(2,3) cases as explained above. They are, thus, not presented.

#### IV. EXPERIMENTAL RESULTS AND DISCUSSIONS

In this section, the traffic noise TL of the plenum windows (a single broadband A-weighted rating) will be

presented in the first place to establish a general picture of how the scatterer arrays affect the traffic noise reduction of the plenum windows. It is followed by a detailed analysis on the spectral characteristics of the sound transmission for deeper understanding of the frequency-sensitive interactions between the scatterers and the acoustic modes within the plenum window voids, which could result in the improvement of sound TL.

The geometry of the present plenum window void is complicated. Analytical formulas for the corresponding eigenfrequencies are also not currently available. To facilitate the analysis on the interactions of bandgaps and the window cavity modes, a simplified approach based on the observations of Tong and Tang<sup>8</sup> is adopted such that these eigenfrequencies, thereafter denoted as  $f_{pq}$ , where  $p$  and  $q$  are non-negative integers, can be approximated. Details are given in the Appendix.

#### A. Traffic noise TL

Figure 7(a) summarizes the  $TL_{tr}$  of the plenum windows tested in the present study. Without the scatterer array in the plenum window, the  $TL_{tr}$  of the plenum window with the narrowest gap is slightly higher, while those of the two other plenum windows are very similar.

In the presence of the scatterers, one can notice that for a fixed  $G$ , the  $TL_{tr}$  tends to increase with increasing scatterer cylinder diameter  $d$  in general regardless of the form of the scatterer array. Also, it is found that for a fixed  $d$ , the plenum window with  $G = 158$  mm in general gives the lowest  $TL_{tr}$ . There appears no clear relationship between  $TL_{tr}$  and

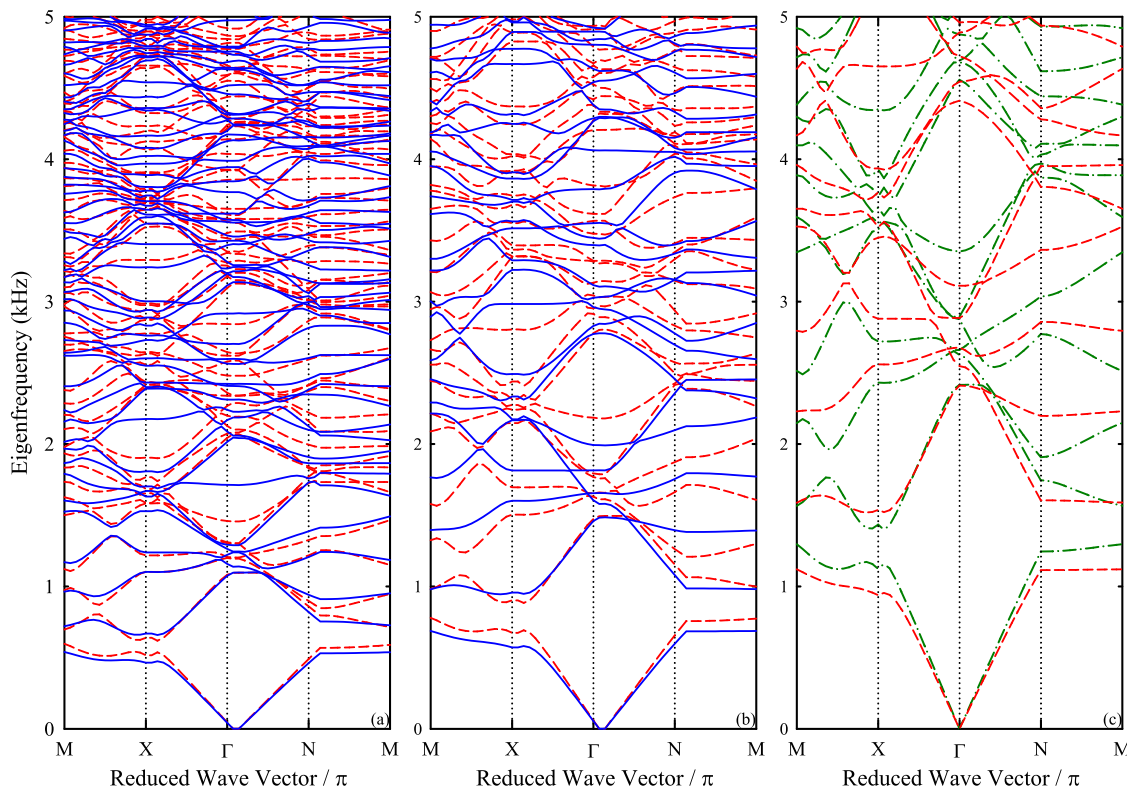


FIG. 6. (Color online) Band structures of the virtual sonic crystals in V(2,3) with rhombic unit cells. Symbols, same as those of Fig. 5.

$d/G$  or the cross section blockage ratio  $nd/G$ . The staggered arrays tend to increase the  $TL_{tr}$ , and the dual staggered arrays give the best performance in general.

Figure 7(b) illustrates the increase in sound TL by installing scatterer arrays into the plenum windows.  $\Delta TL_{tr}$ s of the narrowest windows (with  $G=98$  mm) are in general insignificant when installed with the smallest scatterers ( $d=10$  mm) regardless of the form of the scatterer array. One can also notice that  $\Delta TL_{tr}$ s of the windows with the widest  $G$  are in general the largest when the largest scatterers are used ( $d=32$  mm), no matter what the scatterer array configuration is. This observation tends to imply that blockage ratio is not the prime parameter that controls the sound TL in principle. However, blockage does appear to be important for the single column scatterer arrays [which are the V(1,2) and V(1,3)]. In fact, for the two plenum windows with wider  $G$  and when the scatterer diameter is larger than 19 mm,  $\Delta TL_{tr}$  tends to increase with increasing number of scatterers in the window void. The staggered scatterer arrangement further increases the  $\Delta TL_{tr}$ .

One should note that the application of the normalized traffic noise weighting<sup>21</sup> tends to amplify the  $\Delta TL$  at frequencies around the 1000 Hz 1/3 octave band. Therefore, a weak  $\Delta TL_{tr}$  in Fig. 7(b) does not normally imply poor sound insulation over the whole frequency range of interest. A weak  $\Delta TL_{tr}$  can result if the significant sound TL improvements achieved by installing scatterers fall outside the most emphasized frequency range of the traffic noise weighting. This is likely to happen in the V(2,3) cases as the corresponding significant bandgaps are located at frequencies higher than 1000 Hz (Figs. 5 and 6).

An illustration of the frequency-dependent  $\Delta TL_{23}$  is given in Fig. 8(a). One can observe that improvement of the TL after the installation of the scatterer array is biased to the high frequency end of the frequency range of interest, where bandgaps are found (Fig. 5). The narrower the gap  $G$ , the greater the shift of the TL improvement to the high frequency side ( $f_{B\alpha}$  increases with decreasing  $G$ ). The relatively low  $\Delta TL_{tr,23}$  of the V(2,3) windows with narrow  $G$  and/or small scatterer is due to the property of the normalized traffic noise weighting, which has down-weighted significantly the high frequency TL improvement. However, these windows will still be useful if the noise to be attenuated has significant high frequency content, such as that from commercial aircraft.<sup>29</sup> Also, the results reveal that for a fixed  $G$ , the  $\Delta TL_{23}$  decreases with decreasing  $\sigma$ . One point worthy of note is that  $\Delta TL_{23}$  is very limited around the first Bragg interference frequency in the  $\Gamma X$  direction ( $f_{B1}$ ), but it tends to increase as frequency is increased further. For  $G=218$  mm, the peak  $\Delta TL_{23}$  appears at around  $f_{B3}$ , where a more organized  $\Gamma X$  bandgap is observed [Fig. 5(a)].

For  $G=158$  mm, the observed  $\Delta TL_{23}$  peaks around the 2000 and 4000 Hz frequency bands for  $d=32$  and 19 mm are in line with the complete bandgaps and related band structures observed in Fig. 5(b). The complete bandgap at  $\sim 4000$  Hz for the case of  $G=98$  mm,  $d=19$  mm [Fig. 5(c)] should also contribute to the high  $\Delta TL_{23}$  within the corresponding frequency band.

There are limited low frequency TL variations [Fig. 8(a)] after putting the scatterer arrays into the window void. It is believed that they are due to the window modes whose propagations are not much altered by the sound scattering of

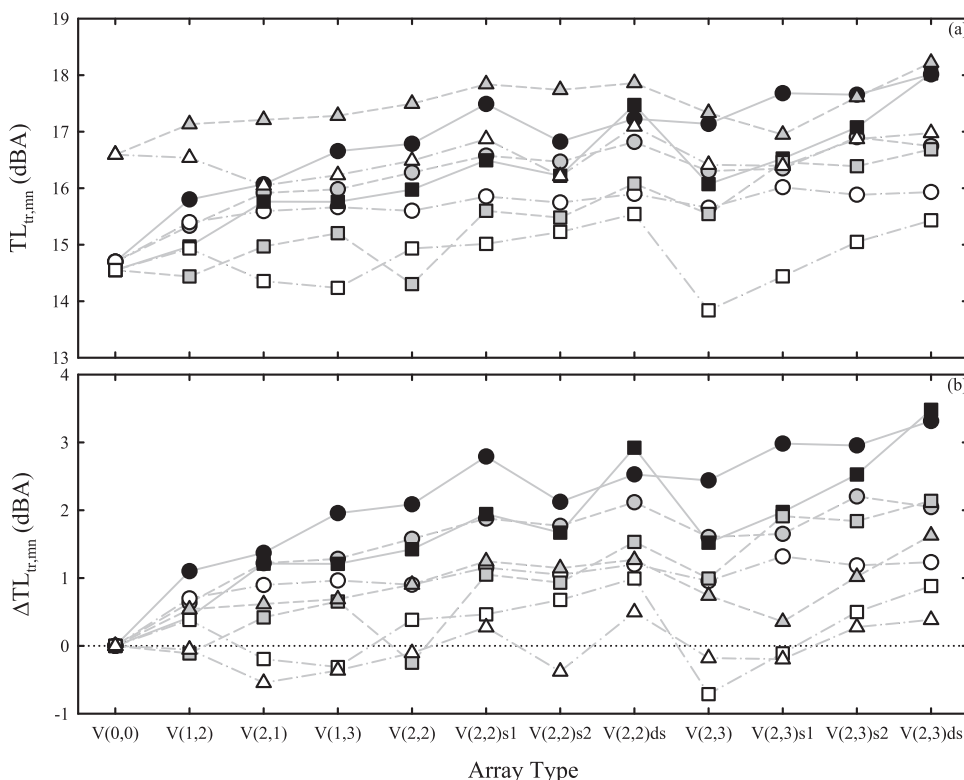


FIG. 7. Traffic noise weighted sound TLs and their changes after the installation of the scatterer arrays. (a)  $TL_{tr,mm}$ ; (b)  $\Delta TL_{tr,mm}$ . Circle,  $G=218$  mm; square,  $G=158$  mm; triangle,  $G=98$  mm. Black,  $d=32$  mm; gray,  $d=19$  mm; white,  $d=10$  mm.



the scatterer array. Some examples of such interactions have been presented in Tang.<sup>15</sup> The spectral characteristics of sound propagation across the plenum windows will be discussed further in Sec. IV B.

It should be noted that the octave band TLs of the plenum windows without the scatterers are reasonably high as shown in Fig. 8(b). The above-observed limited sound amplifications are not significant. One can also notice that the TL spectra tend to shift toward the high frequency end when  $G$  is reduced. The transverse acoustic gap modes have significant influence on the spectral characteristics of the TL<sub>00S</sub>.<sup>15</sup> The first strong TL peaks are due to the first higher cut-off gap mode(s) of the window void ( $f_{01} = c/2G$ ). Close to these frequencies, a large amount of acoustical energy is transferred into these modes, which do not propagate much into the window void. The second TL peak of the window with  $G = 98$  mm seems to be around the eigenfrequency of the second higher odd gap mode ( $f_{03} = 3f_{01}$ ). In fact, a similar observation can be made for the other two windows, but the corresponding second TL peaks are blurred and not as distinctive. Under the current sound incidence condition, the forcing of an even gap mode should be less efficient, and

thus, it is not surprising to find nothing special at those frequencies.

The basic characteristics of the  $\Delta$ TL spectra of the V(1,2), V(2,1), and V(1,3) windows are, in general, in line with those presented in Fig. 8(a) (not shown here). Since the TL improvements achieved by installing these arrays appear to be limited, the corresponding results are not further discussed.

Effects of the scatterers on the TL improvement for the arrays with  $m = 2$  and  $n = 3$  [the V(2,3) series] are summarized in Fig. 9. The data of their non-staggered scatterer counterparts are also included for the sake of easy comparison. For  $G = 218$  mm, the  $\Delta$ TL spectra and their spectral patterns do not vary much for  $d = 10$  and 19 mm [Figs. 9(a) and 9(b)], although the general trend of increasing  $\Delta$ TL with increasing  $d$  is obvious. Relatively strong  $\Delta$ TL dip and peak are observed at the 630 and 1000 Hz one-third octave band, respectively. For the  $d = 32$  mm cases, the staggering tends to enforce strongly the TL peak at around 1000–1250 Hz and, at the same time, reduces the TL at around 630 Hz [Fig. 9(c)].

When  $G$  is reduced to 158 mm, the roughly regular  $\Delta$ TL peaks and tips become much less obvious as can be seen from Figs. 9(d)–9(f), but  $\Delta$ TL in general increases with increasing  $d$  as expected. Again, the spectral variation pattern of  $\Delta$ TL is not much dependent on  $d$ . Strong  $\Delta$ TL is observed between the 1000 and 1600 Hz one-third octave bands for  $d \geq 19$  mm. Although there is no complete bandgap within this frequency range [Fig. 6(b)], the relatively wide bandgaps in various directions could have helped reduce sound transmission.

Further reduction of  $G$  to 98 mm does not greatly improve the  $\Delta$ TL for  $d = 10$  mm. However, one should note that the TL<sub>00</sub> of the  $G = 98$  mm window is, in general, higher than those of the other windows [Fig. 8(b)]. Strong TL improvement is observed at  $d = 19$  mm for frequencies higher than 2000 Hz when the scatterer rows are staggered. In fact, the filing fraction of this setting is similar to that of the case shown in Fig. 9(f). The  $\Delta$ TL peaks in this  $G = 98$  mm are shifted to higher frequency, probably because of band structures of the virtual sonic crystals as discussed in Sec. III and illustrated in Fig. 5(c).

The results of the V(2,2) cases with staggered scatterer rows are presented in Fig. 10. Compared with the results shown in Fig. 9, it is observed that the spectral  $\Delta$ TL patterns of the  $G = 218$  mm gap cases are not much affected by the array lattice, although there is less improvement at the 1000 Hz frequency band in this case [Figs. 10(a)–10(c)]. The  $\Delta$ TL dips and peaks are, therefore, not likely to be due to the band structures of the virtual sonic crystals formed by the scatterers, although one cannot exclude that they could affect the magnitude of the  $\Delta$ TL because of the bandgaps in the MX and NM directions and the narrow  $\Gamma$ X bandgap around 1000 Hz [Fig. 6(a)]. However, the even stronger TL enhancement by the dual staggered scatterers [in V(2,3)ds] observed in Fig. 10(c) could suggest the existence of contributions other than band structures. For the “ds” case, there

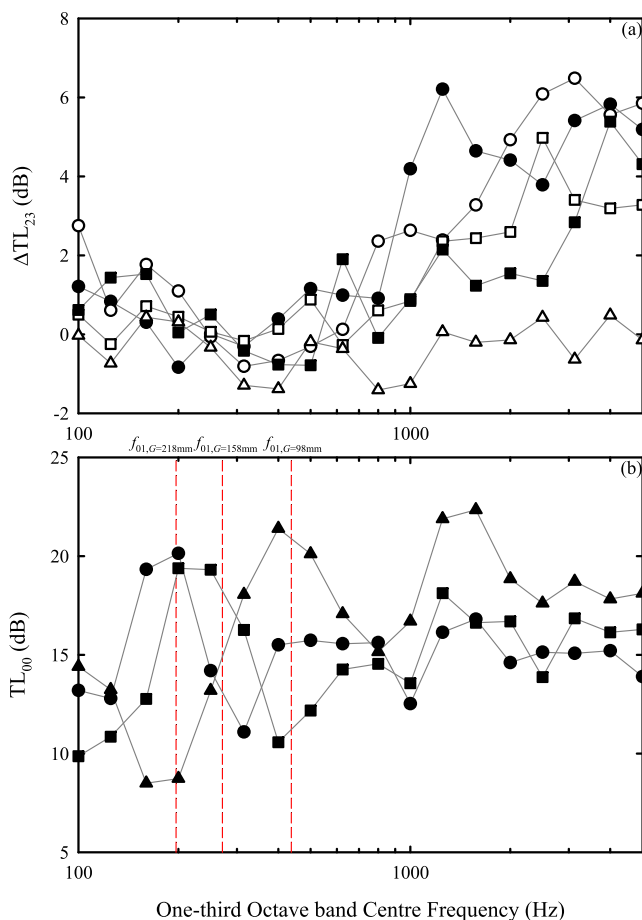


FIG. 8. (Color online) (a) One-third octave band  $\Delta$ TLs of V(2,3) windows.  $\bullet$ ,  $G = 218$  mm,  $d = 32$  mm;  $\blacksquare$ ,  $G = 98$  mm,  $d = 19$  mm;  $\circ$ ,  $G = 158$  mm,  $d = 32$  mm;  $\square$ ,  $G = 158$  mm,  $d = 19$  mm;  $\triangle$ ,  $G = 158$  mm,  $d = 10$  mm. (b) One-third octave band sound TLs of V(0,0) windows.  $\bullet$ ,  $G = 218$  mm;  $\blacksquare$ ,  $G = 158$  mm;  $\blacktriangle$ ,  $G = 98$  mm.

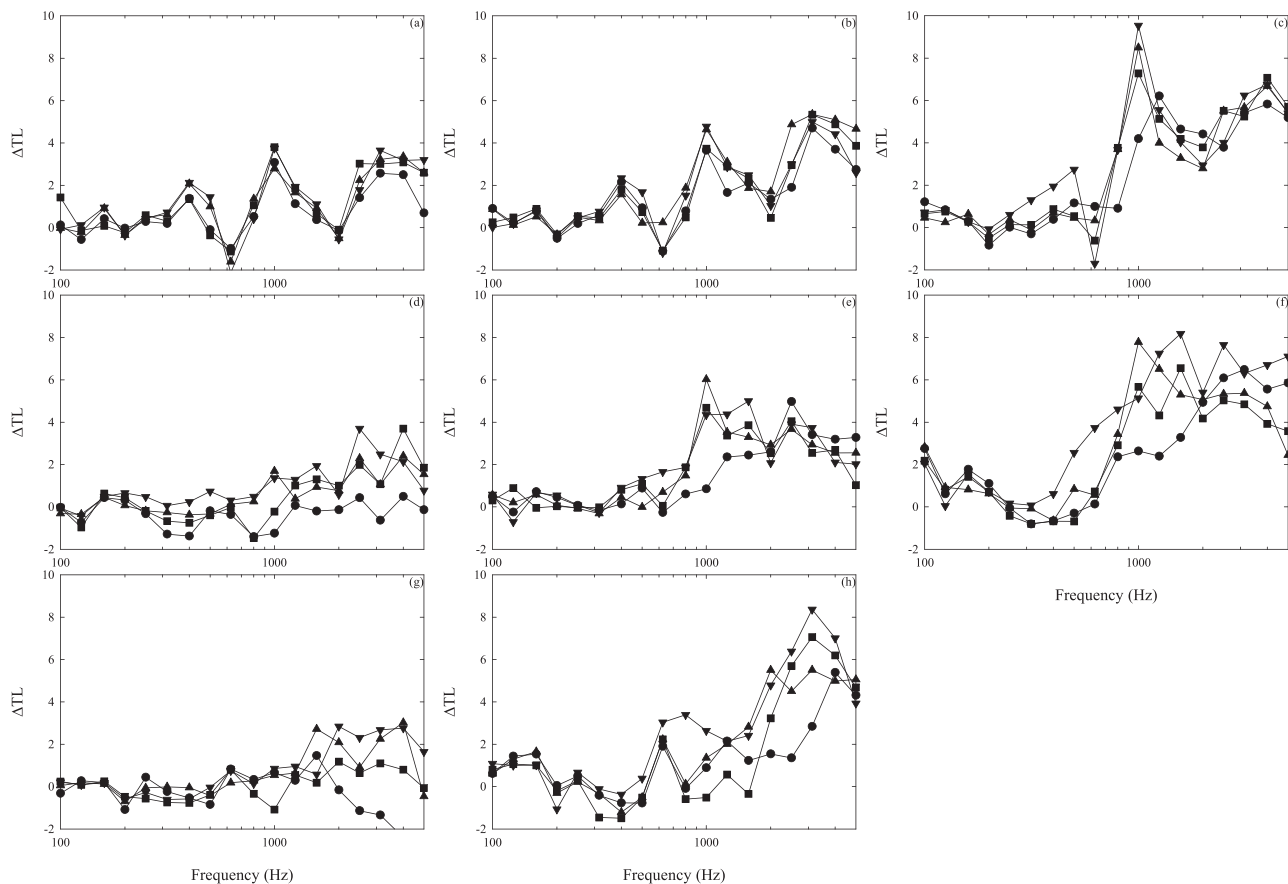


FIG. 9. Effects of scatterer row staggering on TL improvement for V(2,3) window series.  $G = 218$  mm: (a)  $d = 10$  mm; (b)  $d = 19$  mm; (c)  $d = 32$  mm.  $G = 158$  mm: (d)  $d = 10$  mm; (e)  $d = 19$  mm; (f)  $d = 32$  mm.  $G = 98$  mm: (g)  $d = 10$  mm; (h)  $d = 19$  mm.  $\bullet$ , regular/non-staggered;  $\blacksquare$ , s1;  $\blacktriangle$ , s2;  $\blacktriangledown$ , ds.

is basically no bandgap around 1000 Hz [Fig. 5(a)]. This will be discussed further in Sec. IV B.

In general, the  $\Delta TL$ s of the staggered V(2,2) cases are lower than those of their V(2,3) counterparts, except when both  $G$  and  $d$  are small [Figs. 9(g) and 10(g)]. A smaller  $G$  tends to increase the eigenfrequencies of the window gap modes, while a larger scatterer separation tends to lower the band structure eigenfrequencies of the scatterer array. For  $G = 98$  mm,  $f_{B1}$  is near to  $f_{03}$  of the window gap mode for the V(2,2) series. The combined effect of the virtual sonic crystal stop band and the strong evanescent waves around  $f_{03}$  could be the reason for the higher  $\Delta TL$  observed in Fig. 10(g). This phenomenon is likely to be observable for small  $d$  when the blockage due to the installation of scatterers is less serious.

As discussed before, for the scatterer arrays with a rhombic lattice, the complete bandgaps and wider bandgaps in the NM, MX,  $\Gamma X$ , and  $\Gamma N$  directions observed with decreasing  $G$  [Figs. 6(b) and 6(c)] should result in more broadband TL improvement. This is reflected by the results shown in Figs. 10(e)–10(h).

## B. Frequency characteristics of sound transmission

One can notice from the discussions in Secs. III and IV A that the measured TL improvement by installing

scatterer arrays does not always align with the band structure patterns. One plausible reason is certainly the small number of scatterer rows in the present study, such that the sonic crystal bandstop effect is not as strong as expected. It is also believed that the window cavity modes can play an important role in affecting the TL.

Figure 11 illustrates the narrowband TL spectra of the V(0,0) windows. The frequency resolution adopted is 4 Hz. It is the narrowband version of Fig. 8(b). Figure 11(b) gives a better presentation of the TL values at higher frequencies. It is noticed that there is a dip around 130 Hz for all windows, which is probably due to the standing wave between the two window openings. The longitudinal separation between the centres of the two openings in the scale model is around 333 mm, and thus, the fundamental longitudinal resonance frequency should be around 515 Hz, which corresponds to the resonance frequency of 128.8 Hz for the full size window ( $f_{01}$ ).

One can also notice the TL peaks in Fig. 11 are quite broadband. These peaks, especially those below 1000 Hz, are closely related to the standing waves in the gap-wise direction within the overlapping region. For instance, for the  $G = 158$  mm window, the broadband peaks are found centred at  $\sim f_{01}$  ( $\sim 270$  Hz) and  $\sim 2f_{01}$  ( $= f_{02}$ ) and a small relatively sharp peak at  $\sim 3f_{01}$  ( $= f_{03}$ ). A similar phenomenon can be observed for the other two windows basically.

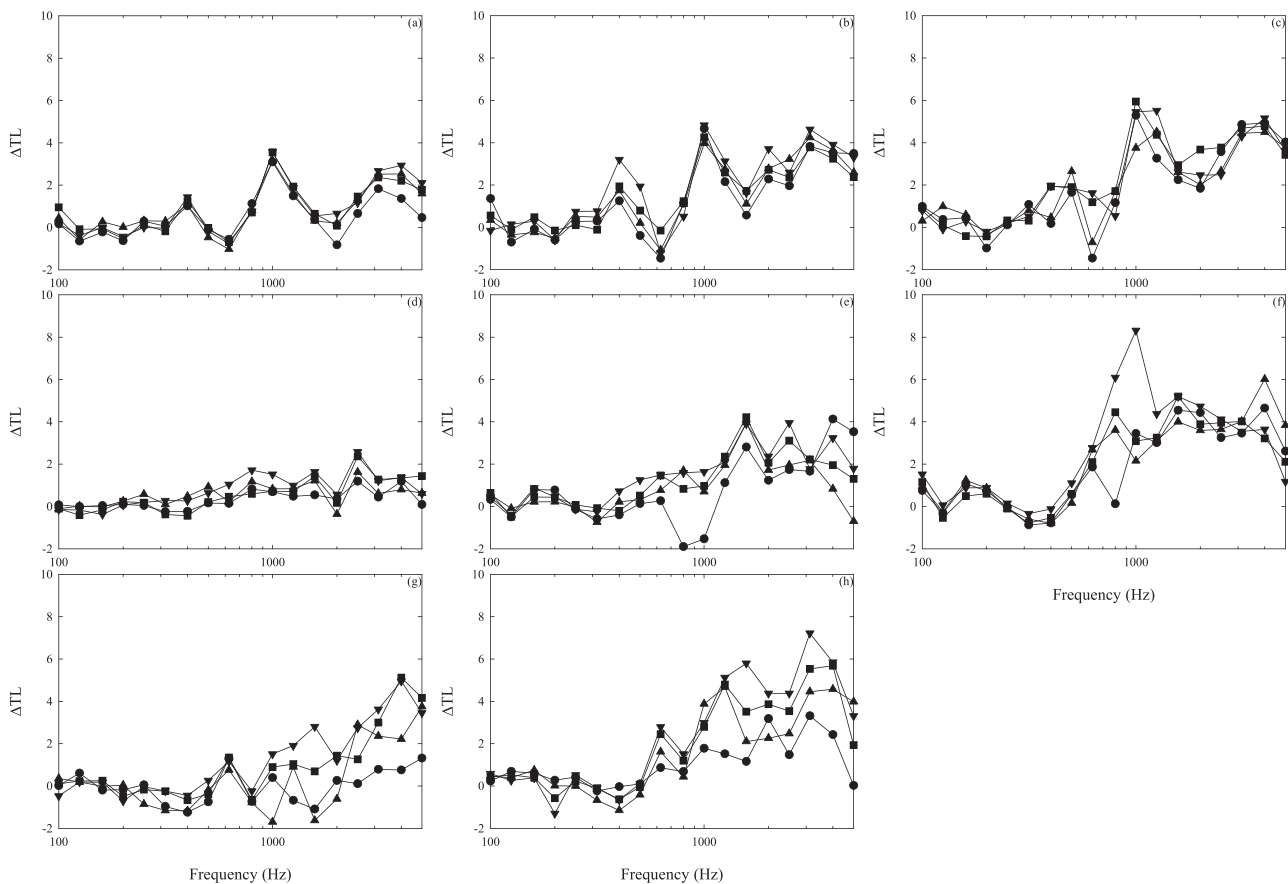


FIG. 10. Effects of scatterer row staggering on TL improvement for V(2,2) window series. Symbols, same as those of Fig. 9.

The broadband nature of these TL peaks is believed to be the result of the multiple coupling between the gap modes and the longitudinal modes within the window void. The existence of these couplings has briefly been illustrated in Tong and Tang.<sup>8</sup>

There is a large TL dip at a frequency of  $\sim 900$  Hz for all windows. While the cause of this dip is not clear, it is interesting to note that the dip is concentrated at a frequency corresponding to the eigenfrequencies of the couple modes formed by the gap modes and longitudinal modes of the same harmonic order. The resonance of the longitudinal modes usually results in lower TL as they tend to create a strong pressure zone at the opening of the window. For  $G = 98$  mm, the dip frequency is around the eigenfrequency of the acoustic mode formed by the coupling of the first harmonics of the gap mode and that of the longitudinal mode ( $f_{22}$ ). For  $G = 158$  and  $218$  mm, it is the second ( $f_{33}$ ) and third harmonics ( $f_{44}$ ), respectively. It is possible that the gap modes can couple with many harmonics of the longitudinal modes (see the Appendix), giving rise to the observed relatively broadband TL dip. The presence of scatterers could adversely affect the formation of these coupled modes and improve very much the TL around this dip frequency. However, the TL peaks could also be reduced because of the interference of the scatterers. One can observe TL peaks around frequencies at higher harmonics of the gap modes as frequency increases, but the variations of the TL appear to

be bounded, and the TLs fluctuate about a certain mean value for each  $G$ . This mean value appears to go higher as  $G$  decreases. There is serious modal overlapping, and thus, the results are not discussed further.

Figure 12 illustrates the spectral variation of TL of the V(2,3) window with  $G = 218$  mm. It should be noted that the virtual sonic crystal at this lattice constant does not give any full bandgap within the frequency range of interest, although there are isolated bandgaps in some particular lattice directions [Fig. 5(a)]. The installation of the  $d = 10$  mm scatterers results in limited TL improvement except at some TL dips of the corresponding V(0,0). Such improvements should be due to the scattering effect of the cylinders, which tends to weaken the resonating cavity modes originally excited within the corresponding V(0,0) window.

The increase in  $d$  to 32 mm results in a broadband TL improvement for frequencies higher than  $\sim 1000$  Hz as shown in Fig. 12(b). While the blockage due to larger  $d$  could be a reason, it is also noticed from Fig. 5(a) that there are quite a number of relative wide bandgaps at frequencies between the TL dips of V(0,0) in various lattice directions. For instance, one can observe this around 1500 Hz in the GX direction and so on.

The blockage resulting from the scatterers in V(2,3) is the same as that in V(2,3)ds, and the corresponding virtual sonic crystals have the same band structure theoretically. However, stronger TL improvement is observed, especially

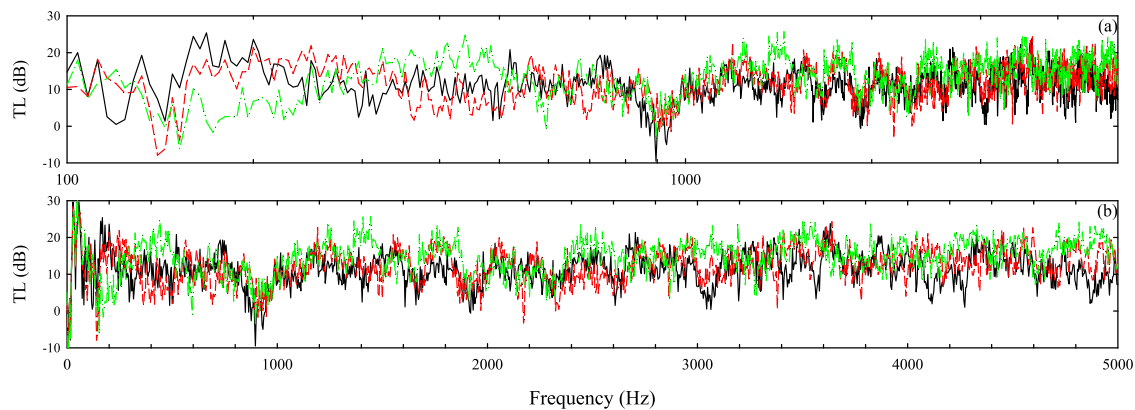


FIG. 11. (Color online) Narrowband spectral variation of TL of V(0,0). (a) Logarithmic frequency axis; (b) linear frequency axis. Solid line,  $G = 218$  mm; dashed line,  $G = 158$  mm; dotted-dashed line,  $G = 98$  mm.

around the TL dip frequencies of V(0,0), as shown in Fig. 12(d). It is, therefore, reasonable to believe that the scatterers attached to the walls have further weakened the gap modes. The resonance of the gap mode results in vanishing normal velocity at the walls, and the hemi-cylindrical scatterers there do not help. The more such cylinders there are on the walls, therefore, the stronger is the weakening effect. This is in line with the TLs of V(2,3)s1 shown in Fig. 12(c).

The virtual sonic crystal in V(2,3)s1 has a rhombic lattice. A full bandgap is observed at the frequency  $\sim 600$  Hz [Fig. 6(a)], but it does not give noticeable TL improvement as can be seen in Fig. 12(c). The low frequency TLs appear to be controlled by the cavity modes of the macroscopic structure V(0,0). Again, one can find bandgaps in different directions of the crystal lattice, which can be the reason for

the broadband TL improvement apart from purely sound blockage. One can observe a relatively longer bandgap at around 2500 Hz for  $d = 32$  mm, which spans along the directions  $\Gamma X$ ,  $\Gamma N$ , and  $NM$  [Fig. 6(a)]. The sharp TL peak close to this frequency observed in Fig. 12(c) could be its consequence. The results of the corresponding V(2,3)s2 are very similar to those presented in Fig. 12(c) and, thus, are not shown here.

In Fig. 13 are presented the TL improvements for the V(2,3) cases of  $G = 158$  mm,  $d = 32$  mm. The TL improvements by installing the scatterers are, in general, in line with those presented in Fig. 12. However, at this lattice constant and scatterer diameter, a full bandgap, although narrow in bandwidth, can be clearly seen at around 2400 Hz [Fig. 5(b)]. There is another relatively long but narrow

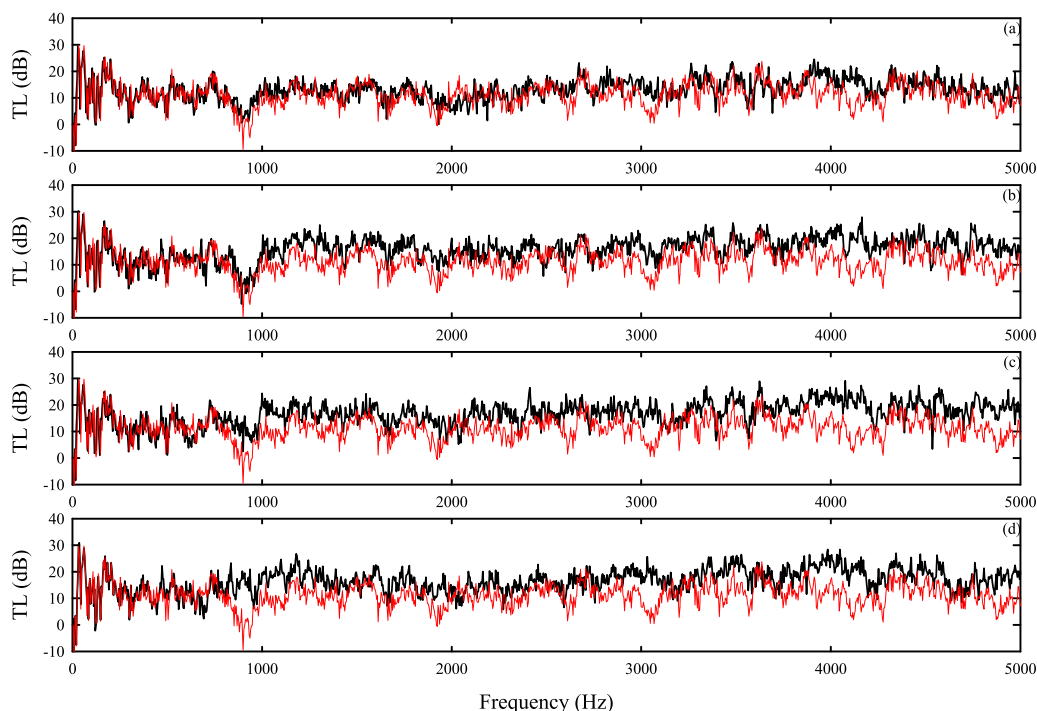


FIG. 12. (Color online) Narrowband spectral variation of TL of V(2,3) with  $G = 218$  mm. (a) V(2,3),  $d = 10$  mm; (b) V(2,3),  $d = 32$  mm; (c) V(2,3)s1,  $d = 32$  mm; (d) V(2,3)ds,  $d = 32$  mm. Thin lines, TL of V(0,0),  $G = 218$  mm.



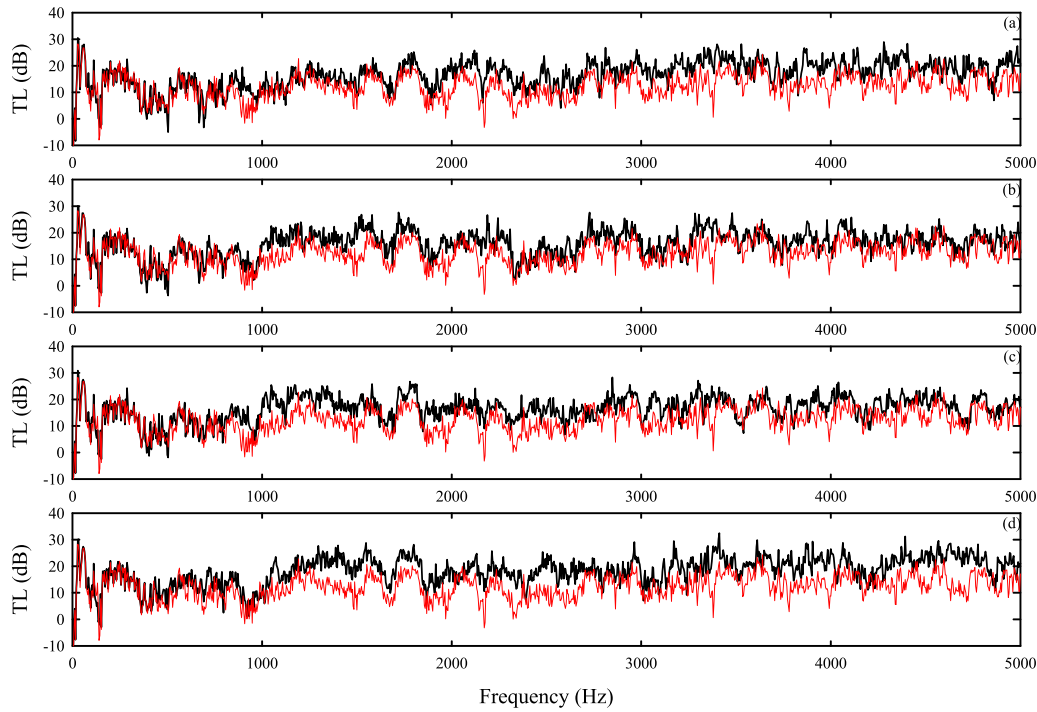


FIG. 13. (Color online) Narrowband spectral variation of TL of the V(2,3) window.  $G = 158$  mm. (a) V(2,3),  $d = 32$  mm; (b) V(2,3)s1,  $d = 32$  mm; (c) V(2,3)s2,  $d = 32$  mm; (d) V(2,3)ds,  $d = 32$  mm. Thin lines, TL of V(0,0),  $G = 158$  mm.

bandgap at around 4000 Hz. The TL improvement by installing regular scatterer arrays [Figs. 13(a) and 13(d)] is, therefore, better than those resulting from arrays with rhombic lattice [Figs. 13(c) and 13(d)] within these frequency ranges in which the latter does not have significantly wide bandgaps [Fig. 6(b)]. On the contrary, the rhombic lattice

[V(2,3)s1 and V(2,3)s2] gives rise to a significant full bandgap at a frequency around 900 Hz, giving rise to the better TL improvement closer to this frequency than the regular lattice cases of V(2,3) and V(2,3)ds.

Figure 14 illustrates the TL spectral variations for the V(2,3) cases with  $d = 19$  mm,  $G = 98$  mm. The window gap

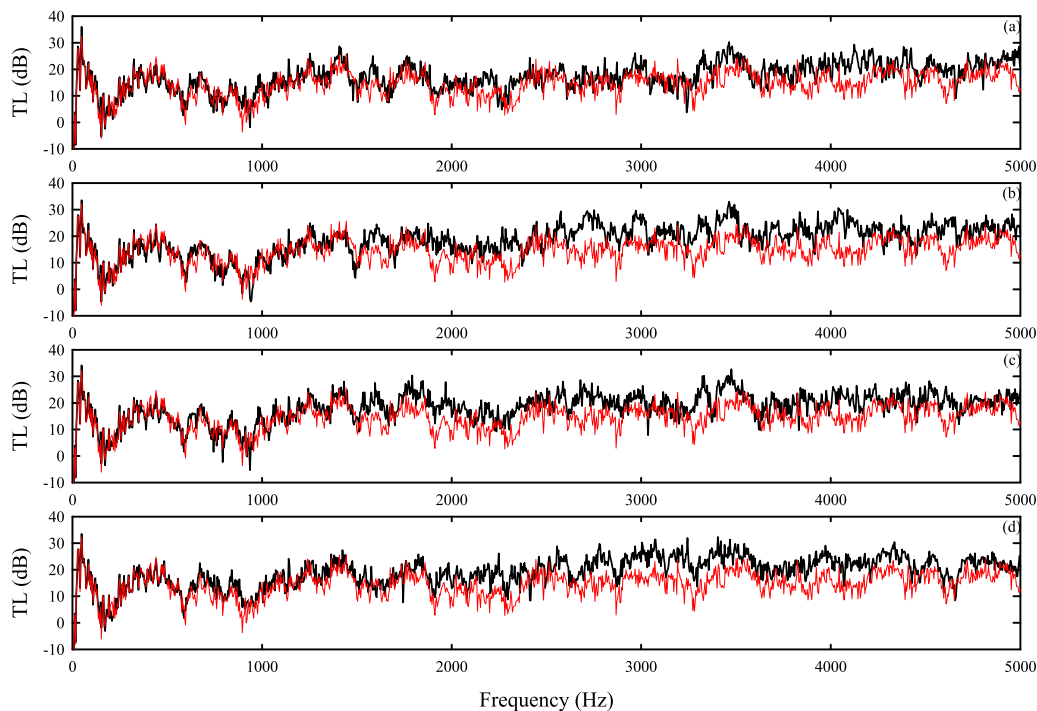


FIG. 14. (Color online) Spectral variation of TL of the V(2,3) window with  $G = 98$  mm. (a) V(2,3),  $d = 32$  mm; (b) V(2,3)s1,  $d = 32$  mm; (c) V(2,3)s2,  $d = 32$  mm; (d) V(2,3)ds,  $d = 32$  mm. Thin lines, TL of V(0,0),  $G = 98$  mm.

width is small. The acoustic modal structures in the window void of the macroscopic  $V(0,0)$  at frequencies below 1500 Hz have stronger integrity such that any bandgap effect of the virtual sonic crystals becomes insignificant within that frequency range. However, the TL improvements by the rhombic lattice arrays [Figs. 14(b) and 14(c)] are still slightly better than those by the regular lattice arrays [Figs. 14(a) and 14(d)] below 2000 Hz, probably due to the full bandgaps of the former [Fig. 6(c)].

The regular lattice scatterer arrays give a full bandgap at around 4000 Hz [Fig. 5(c)]. One can observe significant TL improvements in the proximity of this frequency. However, this effect is only strongly manifested in the case of  $V(2,3)$ ds, where a broadband and relatively uniform TL increase is found [Fig. 14(d)]. There is also considerable TL improvement around 4000 Hz in the cases of  $V(2,3)$ s1 and  $V(2,3)$ s2, but these rhombic lattice arrays do not have such full bandgap at this frequency level, and the frequency range of the improvement is more restricted. It is still unclear how much of a contribution of the full bandgap of the regular lattice array is within the overall TL improvement as the scatterers attached to the wall can also weaken the gap modes (discussed before). Further investigations are required.

The spectral TL improvements in the  $V(2,2)$  cases are basically in line with those in the corresponding  $V(2,3)$  cases, and thus, they are not presented here. However, it should be noted that the eigenfrequencies of the band structures of the  $V(2,2)$  related scatterer arrays are in general  $2/3$  of those of the latter. Therefore, there is a shift of the TL improvements toward the low frequency side of the spectrum, and some lower frequency bandgaps have been ineffective in the presence of the macroscopic  $V(0,0)$  structure cavity modes.

## V. CONCLUSIONS

A scale-down model experiment was carried out in the present study in an attempt to understand how much the sound TL of a plenum window can be improved by installing cylindrical scatterer arrays of different lattices into the window void. In order not to jeopardize the natural ventilation enabling ability of the window, the number of scatterer rows, counted in the direction from the window outdoor opening to the indoor opening, was kept below 3. Three window gap widths and three scatterer diameters were selected for the present parametric study. With acoustically hard window walls, the scatterer arrays resembled virtual sonic crystals. Two lattice structures, namely the regular and the rhombic, were included in the present investigation.

Without the scatterers, the gap modes and the longitudinal modes between the two plenum window openings control the spectral variation of sound TL across the window. The wider the window gap, the better the low frequency performance of the window, but the weaker its protection against traffic noise intrusion.

The installation of the scatterer arrays into the window void in general does help improve the sound TL across the

window. The scatterers weaken the acoustic resonances that result in the strong sound transmission across the original plenum window. Also, the higher the scatterer diameter-to-window gap ratio, the higher the TL in general. However, the arrangement of the scatterers has a crucial effect on the spectral variation of the sound TL. Those arrangements with scatterer(s) attached to the window walls appear to be helpful.

Although the scatterer arrays adopted include a maximum of only two scatterer rows, there is evidence that the bandgaps of these virtual sonic crystals do play a role in shaping the spectral variation of sound TL across the plenum window, unless the frequencies of the bandgaps fall into the low frequency range in which the original cavity modes of the window dominate the sound transmission process. While a full bandgap helps improve sound TL, the present results also tend to suggest that the bandgaps in various lattice directions could have resulted in the broadband improvement of sound TL. However, it is still unclear how significant these bandgaps are in improving the acoustical insulation as the scatterers actually block to some extent the sound propagation path and affect the cavity mode excitations within the window void. This is left to further investigations.

## ACKNOWLEDGMENTS

X.-L.L. and W.K.L. are co-first authors and contributed equally to this work. The financial support of the Research Grants Council, the Hong Kong Special Administration Region Government, China under Project Nos. 152164/15E and 152172/19E, and the Chongqing Postdoctoral Science Foundation (Grant No. cstc2021jcyj-bsh0102) is gratefully acknowledged.

## APPENDIX: EIGENFREQUENCIES OF THE SIMPLIFIED PLENUM WINDOW VOID

One can observe from the simulation of Tong and Tang<sup>8</sup> under normal sound incidence that the standing wave patterns inside the window void are basically made up of the gap modes and the longitudinal plane wave modes along the length of the plenum window. The former give rise to standing wave patterns parallel to the windowpanes. The latter match better those modes with relatively strong sound pressure regions near the window inlet and outlet. The longitudinal distance between the centres of these two window openings is  $2L/3$  in the present study.

Let  $p$  and  $q$  be the mode orders of the longitudinal modes and the gap modes, respectively; the eigenfrequencies of the window cavity modes,  $f_{pq}$ , can then be approximated as

$$f_{pq} \approx \frac{c}{2} \sqrt{\left(\frac{p}{2L/3}\right)^2 + \left(\frac{q}{G}\right)^2}. \quad (\text{A1})$$

Table 1 presents the  $f_{pq}$ s for  $p \leq 6$  and  $q \leq 4$ . These frequencies are scaled back to those for the full size practical window. Larger  $p$  is not meaningful as too short a wavelength

TABLE I.  $f_{pg}$ s of the simplified plenum window cavity.

$p$	$q$												
	All $G$ s	$G = 98 \text{ mm}$				$G = 158 \text{ mm}$				$G = 218 \text{ mm}$			
	0	1	2	3	4	1	2	3	4	1	2	3	4
0	0.0	437.5	875.0	1312.5	1750.0	271.4	542.7	814.1	1085.4	196.7	393.3	590.0	786.7
1	128.8	456.1	884.4	1318.8	1754.7	300.4	557.8	824.2	1093.1	235.1	413.9	603.9	797.2
2	257.5	507.7	912.1	1337.5	1768.8	374.1	600.7	853.8	1115.6	324.0	470.1	643.8	827.8
3	386.3	583.6	956.5	1368.2	1792.1	472.1	666.1	901.1	1152.1	433.4	551.3	705.2	876.4
4	515.0	675.8	1015.3	1409.9	1824.2	582.1	748.2	963.3	1201.4	551.3	648.0	783.2	940.3
5	643.8	778.4	1086.3	1461.9	1864.7	698.6	842.0	1037.9	1262.0	673.1	754.4	873.2	1016.5
6	772.5	887.8	1167.2	1523.0	1912.9	818.8	944.1	1122.3	1332.3	797.2	866.9	972.1	1102.6

compared to the window opening does not guarantee a fairly uniform sound pressure region in the proximity of the opening.

<sup>1</sup>O. Hänninen, A. B. Knol, M. Jantunen, T. A. Lim, A. Conrad, M. Rappolder, P. Carrer, A. C. Fanetti, R. Kim, J. Buekers, R. Torfs, I. Iavarone, T. Classen, C. Hornberg, O. C. L. Mekel, and the EBoDE Working Group, "Environmental burden of disease in Europe: Assessing nine risk factors in six countries," *Environ. Health Perspect.* **122**, 439–446 (2014).

<sup>2</sup>WHO Regional Office for Europe, *Burden of Disease from Environmental Noise – Quantification of Healthy Life Years Lost in Europe*, edited by L. B. A. Fritsch, A. L. Brown, R. Kim, D. Schwela, and S. Kephelopoulous (World Health Organization, Geneva, Switzerland, 2011).

<sup>3</sup>U. J. Kurze, "Noise reduction of barriers," *J. Acoust. Soc. Am.* **55**, 504–518 (1974).

<sup>4</sup>E. Öhrström, A. Skånberg, H. Svensson, and A. Gidlöf-Gunnarsson, "Effects of road traffic noise and the benefit of access to quietness," *J. Sound Vib.* **295**, 40–59 (2006).

<sup>5</sup>D. N. May, "Freeway noise and high-rise balconies," *J. Acoust. Soc. Am.* **65**, 699–704 (1979).

<sup>6</sup>A. J. B. Tadeu and D. M. R. Mateus, "Sound transmission through single, double and triple glazing," *Exp. Eval. Appl. Acoust.* **62**, 307–325 (2001).

<sup>7</sup>S. K. Tang, "A review on natural ventilation-enabling façade noise control devices for congested high-rise cities," *Appl. Sci.* **7**, 175 (2017).

<sup>8</sup>Y. G. Tong and S. K. Tang, "Plenum window insertion loss in the presence of a line source—A scale model study," *J. Acoust. Soc. Am.* **133**, 1458–1467 (2013).

<sup>9</sup>Y. G. Tong, S. K. Tang, J. Kang, A. Fung, and M. K. L. Yeung, "Full scale field study of sound transmission across plenum windows," *Appl. Acoust.* **89**, 244–253 (2015).

<sup>10</sup>X. L. Li, S. K. Tang, S. Y. C. Yim, R. Y. C. Lee, and T. Hung, "Noise reduction of plenum windows on the façade of a high-rise residential building next to heavy road traffic," *Build. Environ.* **186**, 107353 (2020).

<sup>11</sup>R. D. Ford and G. Kerry, "The sound insulation of partially open double glazing," *Appl. Acoust.* **6**, 57–72 (1973).

<sup>12</sup>X. Yu, S. K. Lau, L. Cheng, and F. Cui, "A numerical investigation on the sound insulation of ventilation windows," *Appl. Acoust.* **117**, 113–121 (2017).

<sup>13</sup>L. Du, S. K. Lau, and S. E. Lee, "Experimental study on sound transmission loss of plenum window," *J. Acoust. Soc. Am.* **146**, EL489–EL495 (2019).

<sup>14</sup>J. Kang and B. M. Brocklesby, "Feasibility of applying micro-perforated absorbers in acoustic window systems," *Appl. Acoust.* **66**, 669–689 (2005).

<sup>15</sup>S. K. Tang, "Reduction of sound transmission across plenum windows by incorporating an array of rigid cylinders," *J. Sound Vib.* **415**, 25–40 (2018).

<sup>16</sup>H. M. Lee, Z. Wang, K. M. Lim, J. Xie, and H. P. Lee, "Novel plenum window with sonic crystals for indoor noise control," *Appl. Acoust.* **167**, 107390 (2020).

<sup>17</sup>H. H. El Dien and P. Woloszyn, "The acoustical influence of balcony depth and parapet form: Experiments and simulations," *Appl. Acoust.* **66**, 533–551 (2005).

<sup>18</sup>DIRAC, *Dual Input Room Acoustics Calculator User Manual* (Acoustics Engineering, Nærum, Denmark, 2002), pp. 17–19.

<sup>19</sup>C. M. Harris, *Handbook of Noise Control*, 2nd ed. (McGraw Hill, New York, 1979), Chap. 24.

<sup>20</sup>ISO 10140-2, "Acoustics—Laboratory measurement of sound insulation of building elements—Measurement of airborne sound insulation" (International Organization for Standardization, Geneva, Switzerland, 2021).

<sup>21</sup>BS EN 1793-3, "Road traffic noise reducing devices—Test methods for determining the acoustic performance—Part 3. Normalized traffic noise spectrum" (International Organization for Standardization, Geneva, Switzerland, 1998).

<sup>22</sup>M. Garai and P. Guidorzi, "European methodology for testing the airborne sound insulation characteristics of noise barriers *in situ*: Experimental verification and comparison with laboratory data," *J. Acoust. Soc. Am.* **108**, 1054–1067 (2000).

<sup>23</sup>T. Miyashita, "Sonic crystals and sonic wave-guides," *Meas. Sci. Technol.* **16**, R47–R63 (2005).

<sup>24</sup>F. Koussa, J. Defrance, P. Jean, and P. Blanc-Benon, "Acoustical efficiency of a sonic crystal assisted noise barrier," *Acta Acust. united Acust.* **99**, 399–409 (2013).

<sup>25</sup>C. Lagarrigue, J. P. Groby, and V. Tournat, "Sustainable sonic crystal made of resonating bamboo rods," *J. Acoust. Soc. Am.* **133**, 247–254 (2013).

<sup>26</sup>M. Makwana, T. Antonakakis, B. Mailing, S. Guenneau, and R. V. Craster, "Wave mechanics in media pinned at Bravais lattice points," *SIAM J. Appl. Math.* **76**, 1–26 (2016).

<sup>27</sup>J. V. Sánchez-Pérez, D. Caballero, R. Martínez-Sala, C. Rubio, J. Sánchez-Dehesa, F. Meseguer, J. Llinares, and F. Gálvez, "Sound attenuation by a two-dimensional array of rigid cylinders," *Phys. Rev. Lett.* **80**, 5325–5328 (1998).

<sup>28</sup>D. P. Elford, L. Chalmers, F. V. Kusmartsev, and G. M. Swallowe, "Matryoshka locally resonant sonic crystal," *J. Acoust. Soc. Am.* **130**, 2746–2755 (2011).

<sup>29</sup>S. Khardi, "Reduction of commercial aircraft noise emission around airports. A new environmental challenge," *Eur. Transp. Res. Rev.* **1**, 175–184 (2009).